Reconstructing Ridge Frequency Map from Minutiae Template of Fingerprints

Wei Tang, Yukun Liu
College of Measurement & Control Technology and Communication Engineering
Harbin University of Science and Technology, Harbin, China, 150080.
{tangwei,liuyukun}@hrbust.edu.cn

Abstract

The fingerprint ridge structure can be directly generated from its following features: the position of minutiae, the orientation field and the ridge frequency map. It was once believed that minutiae template does not reveal sufficient information of the orientation field and ridge frequency map to allow the reconstruction of the original fingerprint image. This belief has now been shown to be false; several algorithms have been proposed to generate the fingerprint ridge structure with uniform ridge frequency by reconstructing the orientation field from minutiae template. However, these reconstruction techniques assume equal ridge frequency in the whole foreground, which results in generating spurious minutiae along the changes of ridge curvature. In this paper, a novel algorithm for reconstructing the ridge frequency map from the minutiae template is proposed to complete the last piece of features required for the reconstruction of fingerprints. The change of local ridge frequency can be perfectly modeled by the minutiae and the divergence of the vectorial orientation field. The reconstructed ridge frequency map has been evaluated to be highly correlated to the ridge frequency map estimated from the original fingerprint images.

1. Introduction

Fingerprints are the most widely used among all biometric recognition systems. The automatic fingerprint recognition system captures a digital representation (image sample) of biometric characteristics for a fingerprint. In order to facilitate matching or comparison, the raw digital representation is usually processed by a feature extractor to generate a compact but expressive representation, called a feature set. The features extracted can be texture-based, such as ridge orientation and frequency information, or minutiae-based, such as ridge endings and bifurcations and their associated ridge flow fragment information. For many years, researchers assume that the minutiae do not contain enough information of texture-based features for the whole image. In other words, the original fingerprint cannot be reconstructed from the positions and directions of minutiae. However, some recent published works [10] [3] [6] [8] have shown that it is possible to reconstruct a fingerprint image from the minutiae to attack the fingerprint recognition system. As a major result, their works proved that the global orientation field is reconstructible from the minutiae. Actually, the orientation field is one of the three fundamental features to generate the original fingerprint image besides of minutiae and ridge frequency map [3]. Consequently, the improvement on the orientation field estimation brings better reconstructed fingerprint images [6]. However, in the above mentioned works of fingerprint reconstruction, the local ridge structure models proposed to generate the local ridge flow enroll a constant ridge frequency value throughout the image. A side effect is that spurious minutiae arouse at the termination points of the generated ridges due to the local frequency constraint when adjacent ridges are concerned. The spurious minutiae were not able to be removed by global optimization operation performed in [10] [6]. Li et al. [8] proposed to remove the spurious minutiae in the continuous phase image. However, the side effect of this operation is that it randomly alters the local ridge structure and thus brings discontinuous ridge spacing.

As one of the fundamental features for fingerprint reverse engineering, the ridge frequency map is still believed to be not reconstructible from minutiae. In this paper, we challenge this perceiving by proposing a novel algorithm reconstructing the ridge frequency map from minutiae directions and positions. The rest of this paper is organized as follows. In section 2, the definition of the local ridge frequency of fingerprint image is reviewed. In section 3, the stable area in which the ridge frequency changes smoothly is analyzed, and the quantization of frequency changes in this kind area is derived. In section 4, the effect of minutiae on the change of local ridge frequency is analyzed and quantized. In section 5, a novel algorithm is described to reconstruct the ridge frequency map from the minutiae template. In section 6, experiments are carried out to validate the proposed algorithm. Finally, some conclusions are drawn and

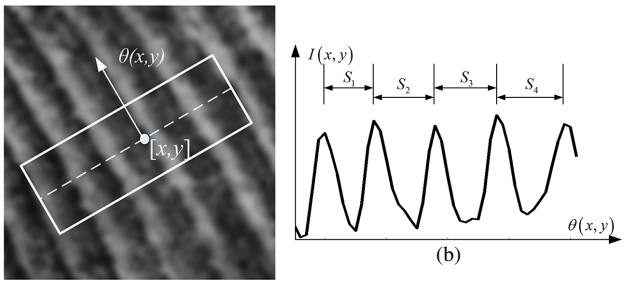

Figure 1. The definition of ridge frequency. (a) The hypothetical segment in the gray scale image at $[x, y]$, with the local ridge orientation $\theta(x, y)$; (b) The distance between the adjacent peaks of pixel intensity value is considered as the space between ridges.

the possible applications of this work is discussed.

2. The definition of local ridge frequency

The local ridge frequency (or density) $f(x, y)$ at point $[x, y]$ is the multiplicative inverse of the distance S between two neighboring ridges, along an orientation orthogonal to the local ridge orientation $\theta(x, y)$ [9]. In practice, it is an average value by estimating the number of ridges K per unit length S along a hypothetical segment centered at $[x, y]$ along $\theta(x, y) + \frac{\pi}{2}$, as shown in Fig.1:

$$f(x, y) = \frac{K}{S} \qquad S = \sum S_n \tag{1}$$

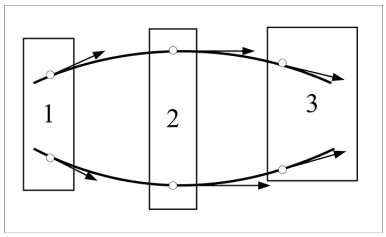

Figure 2. Three cases of local ridge frequency changing tendencies. The first case shown in the box labeled as 1. The directions of two points on the ridgelines indicates the flow is going outward, the space between ridgelines is expanding. The directions of the two points shown in the box label as 2 are identical to each other, indicating the ridgelines are parallel. The Third case shown in the box labeled as 3, which is opposite to case 1. The ridge lines are going inward, the space between ridgelines is decreasing.

3. Ridge frequency in area without minutiae

In a closed area without minutiae, the distance between two ridges changes smoothly. The ridge lines have three possible local ridge frequency changing tendencies, as shown in Fig.2. Here we begin with the first case, which indicates

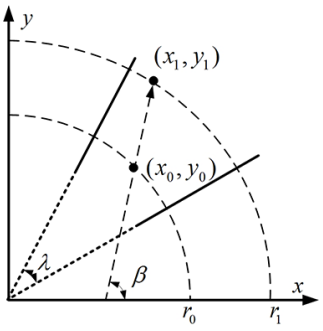

Figure 3. A local field which is modeled by Equation 2 and 3. The solid lines are ridge lines in the small local field.

the space between two ridge lines increases linearly. The local orientation field between the two ridge line fragments can be approximately modeled by a 2D vector field $O(x, y)$:

$$O(x, y) = \begin{pmatrix} x \cdot r^{-1}(x, y) \\ y \cdot r^{-1}(x, y) \end{pmatrix} = \begin{pmatrix} U(x, y) \\ V(x, y) \end{pmatrix} \tag{2}$$

$$r(x, y) = \sqrt{x^2 + y^2} \tag{3}$$

which is actually the gradient field of the 2D density function $r(x, y)$. The origin of $r(x, y)$ is the intersection point of the extension of the two ridge line fragments, as shown in Fig.3. It can be noticed that each points on the circle $r(x, y) = R$ have equal ridge frequency. Suppose the angle between these two ridge line fragments is denoted by λ, the ridge frequency on a point $[x, y]$ in this local area can be given by:

$$f(x, y) = \frac{K}{S} = [2r(x, y) \sin \frac{\lambda}{2}]^{-1} \tag{4}$$

Consider two points $[x_0, y_0]$ $[x_1, y_1]$, as shown in Fig.3, in this local vector field:

$$\begin{pmatrix} x_1 \\ y_1 \end{pmatrix} = \begin{pmatrix} x_0 \\ y_0 \end{pmatrix} + \Delta r \begin{pmatrix} \cos \beta \\ \sin \beta \end{pmatrix} \tag{5}$$

$$\Delta r = \sqrt{(x_1 - x_0)^2 + (y_1 - y_0)^2} \tag{6}$$

The local ridge frequency on these points are $f(x_0, y_0)$ and $f(x_1, y_1)$. According to Equation 4, they have the relation that:

$$f(x_1, y_1) = \frac{r(x_0, y_0)}{r(x_1, y_1)} f(x_0, y_0) \tag{7}$$

According to Equation 5 and 6, it can be derived that:

$$r(x_0, y_0) = \sqrt{(x_1 - \Delta r \cos \beta)^2 + (y_1 - \Delta r \sin \beta)^2}$$

$$= \sqrt{r^2(x_1, y_1) - 2\Delta r(x_1 \cos \beta + y_1 \sin \beta) + \Delta r^2}$$

$$= \sqrt{r^2(x_1, y_1) - 2r(x_1, y_1)\Delta r \cos(\alpha - \beta) + \Delta r^2} \quad (8)$$

where:

$$\alpha = arg(x_1, y_1) \quad (9)$$

is the angle of the vector $O(x_1, y_1)$. So that:

$$\frac{r(x_0, y_0)}{r(x_1, y_1)} = \sqrt{1 - \frac{2\Delta r}{r(x_1, y_1)} \cos(\alpha - \beta) + \frac{\Delta r^2}{r^2(x_1, y_1)}}$$

$$= \sqrt{1 + 2div(x_1, y_1)\Delta r \cos(\alpha - \beta) + div^2(x_1, y_1)\Delta r^2}$$

$$= \Theta(x_1, y_1) \quad (10)$$

where $div(x, y)$ is the divergence of the local vector field $O(x, y)$:

$$div(x, y) = \frac{\partial U}{\partial x} + \frac{\partial V}{\partial y}$$

$$= [r^{-1}(x, y) - 3x^2 r^{-3}(x, y)] + [r^{-1}(x, y) - 3y^2 r^{-3}(x, y)]$$

$$= -r^{-1}(x, y) \quad (11)$$

Then Equation 7 can be expressed by:

$$f(x_1, y_1) = \Theta(x_1, y_1) f(x_0, y_0) \quad (12)$$

It can be derived that Equation 12 also holds for the other two cases shown in Fig.2. The local vector field $O(x, y)$ whose element is within the range $[0, 2\pi)$ is obtained by unwrapping the local orientation field $\theta(x, y)$ whose element is within the range $[0, \pi)$.

Equation 12 gives the change ratio of ridge frequency along an arbitrary direction β with an arbitrary small step Δr. In the case of fingerprint image, the pixels or blocks are aligned vertically and horizontally, which simplifies Equation 12 by letting $\Delta r = 1$, $\beta \in \{0, \frac{\pi}{2}, \pi, \frac{3}{2}\pi\}$.

4. Ridge frequency in area with minutiae

A minutia is either a ridge ending or a ridge bifurcation with their attributes of position $[x, y]$ and direction α, as shown in Fig.4. The type of minutia can alter from ending to bifurcation when the pressure pushed against the sensor increases or the density value of the image is inverted. The alterability of ridge endings and bifurcations suggests that they have equal affect on the local ridge frequency. Therefore, we consider all minutiae are ridge endings for simplification.

A ridge terminates at a minutia point. It results in the ridge frequency changes abruptly along the minutia direction. Without considering the effect of ridge flow given in Equation 12 , according to the definition of ridge frequency as shown in Equation 1:

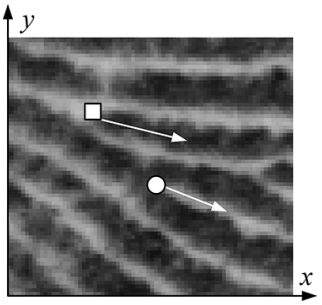

Figure 4. The definition of minutiae. The square denotes the ridge bifurcation and the circle denotes the ridge ending, if the bright pixels are considered as ridge peaks. The bifurcation becomes an ending if the dark pixels are considered as ridge peaks.

$$f(x_1, y_1) = \frac{K - 1}{S} = f(x_0, y_0) - S^{-1} \quad (13)$$

where point $[x_1, y_1]$ is on the vanished ridge line and next to the minutia $[x_0, y_0]$, S is a fixed length for the window size. In order to quantize the affected range S, the intrinsic coordinate system used for minutiae alignment proposed in [2] is adopted in this paper. Taking a minutia as the origin, a minutia intrinsic coordinate system (MICS) can be constructed. The MICS for the i-th minutia is denoted by Ω_i. Ω_i has with two axes, which run along hypothetical lines parallel and perpendicular to the ridge orientations, denoted by $A_i^{\parallel}$ and $A_i^{\perp}$, respectively, as shown in Fig.5. The positive axes, denoted by $A_i^{\parallel +}$ and $A_i^{\perp +}$, start from the origin with the direction α_i and $\alpha_i - \frac{\pi}{2}$, respectively. The valid range of $A_i^{\perp}$ is decided by two points $I_i^{\perp +}$ and $I_i^{\perp -}$. $I_i^{\perp +}$ is the first intersection point with $A^{\parallel +}$ of other MICSs when $A_i^{\perp +}$ is extending from the origin. $I_i^{\perp -}$ is the first intersection point with $A^{\parallel +}$ of other MICSs when its negative part extending from the origin. It is obvious that the length of $A_i^{\perp}$ is the quantization of the affected range S appeared in Equation 13.

A region is called a Stable Area (SA), if it is enclosed by four arbitrary axes $A_i^{\parallel +}$ $A_j^{\parallel +}$ $A_m^{\perp}$ $A_n^{\perp}$, and has no minutia in it. It is denoted by Γ. In fact, the whole foreground can be divided into a number of non-overlapping SAs. Within each SA, the ridges are continuous with no terminations so that Equation 12 can be applied. When tracing from one SA into another, the change of ridge frequency is a combinational effect of Equation 12 and 13:

$$f(x_1, y_1) = \Theta(x_1, y_1) f(x_0, y_0) + \zeta l^{-1}(A_i^{\perp}) \quad (14)$$

where $[x_0, y_0]$ and $[x_1, y_1]$ are two points in Γ_m and Γ_n respectively, $l^{-1}(A_i^{\perp})$ is the valid length of $A_i^{\perp}$ and the value of ζ is decided by the locations of $[x_0, y_0]$ and $[x_1, y_1]$:

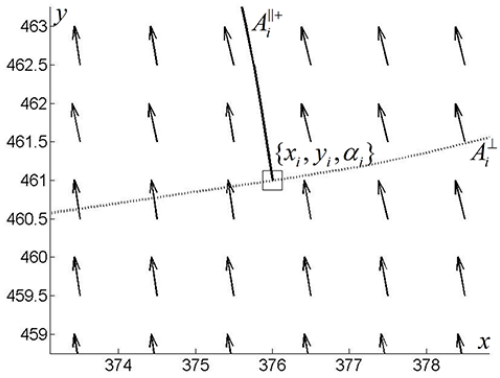

Figure 5. An example of MICS in a local field. The square indicates the position of a minutia, the arrows represent the unwrapped orientation field according to the direction of the minutia. $A_i^{\|+}$ is the solid line. $A_i^{\perp+}$ is the dashed line.

1. $\zeta = -1$, if Γ_m and Γ_n are separated by $A_i^{\perp}$, $A^{\|+}$ is a boundary of Γ_m;
2. $\zeta = 1$, if Γ_m and Γ_n are separated by $A_i^{\perp}$, $A_i{}^{\|+}$ is a boundary of Γ_n;
3. $\zeta = 0$, if Γ_m and Γ_n are separated by $A^{\|+}$;

5. The ridge frequency map reconstruction algorithm

Given a set of N fingerprint minutiae $\{x_n, y_n, \alpha_n\}$, $1 \leq n \leq N$, where (x_n, y_n) and α_n denote the location and direction of the n-th minutiae, respectively, the goal is to reconstruct the original ridge frequency map of the fingerprint.

The local vector field $O(x, y)$ required for Equation 12 is unwrapped from the local orientation field $\theta(x, y)$, which is unknown so far. Therefore, the orientation field $\theta(x, y)$ should be reconstructed in advance. In recent published works, there are numbers of algorithms proposed for reconstructing $\theta(x, y)$ from minutiae. The method of Hill [7] generated the orientation field based on singular points according to the model in [11]. To relieve the dependence on singular points, Ross [10] proposed an orientation field estimation method by averaging the directions of minutiae triplets. Feng [6] improved the averaged orientation of a local point by considering its nearest neighboring minutiae from eight directions. While Cappelli et al. [3] fitted a modified model proposed in [13] to the minutiae directions to achieve a globally optimized orientation field. Here in this paper, the orientation field reconstruction algorithm proposed by Feng [6] is adopted because of its succinctness and flexibility. The algorithm for reconstructing the ridge frequency map can be depicted as follows:

1. Reconstruct the pixel-wise orientation field;
2. Partition the foreground into SAs using the MICSs;
3. Select the left-top pixel in the foreground, which locates in Γ_1, set an initial frequency value $f_0 = 0.12$ to it, use Equation 12 to calculate the ridge frequency values for all other pixels in Γ_1;
4. Select another Γ_i, which is adjacent to the previous processed one;
5. Starting a queue containing all pixels in Γ_i, in each iteration:
   (a) A pixel is obtained from the queue and each of its four-connected neighbors is checked if it has been reconstructed;
   (b) If one of the neighbor pixels is reconstructed, the ridge frequency value of this pixel is estimated according to Equation 14 by considering the location of the neighboring pixel;
   (c) Deleted current pixel from the queue;
   (d) The procedure is repeated until the queue is empty;
6. Repeat step (4) and (5) until all foreground pixels are processed.

The second step in which the foreground is partitioned by the MICSs involves a local orientation unwrapping and implemented by a streamline drawing algorithm [12]. Given an orientation field $\theta(x, y)$ and a minutia $\{x_i, y_i, \alpha_i\}$, the partition algorithm can be depicted as follows:

1. Set the seed point P at $[x_i, y_i]$, the reference direction γ is α_i ;
2. The local orientation field with the window size of 3 by 3 centered at P is unwrapped to $\theta'(x, y)$ in the range $[0, 2\pi)$. The result is that the absolute differences between γ and all orientation elements in the local window are less then $\frac{\pi}{2}$;
3. Draw the streamline according to $\theta'(x, y)$ until the border of the local window is met, record the position $[x_e, y_e]$ and direction $\theta'(x_e, y_e)$ of the end point of the streamline;
4. Update P with the position $[x_e, y_e]$ and γ with $\theta'(x_e, y_e)$;
5. Repeat step (2)(3)(4) until a minutia or the border of the foreground is met.

The streamline starting from minutia $\{x_i, y_i, \alpha_i\}$ and coinciding with $\theta(x, y)$ corresponds to $A_i^{\|+}$. Similarly, $A_i^{\perp+}$ and $A_i^{\perp-}$ can be drawn by the same algorithm as described

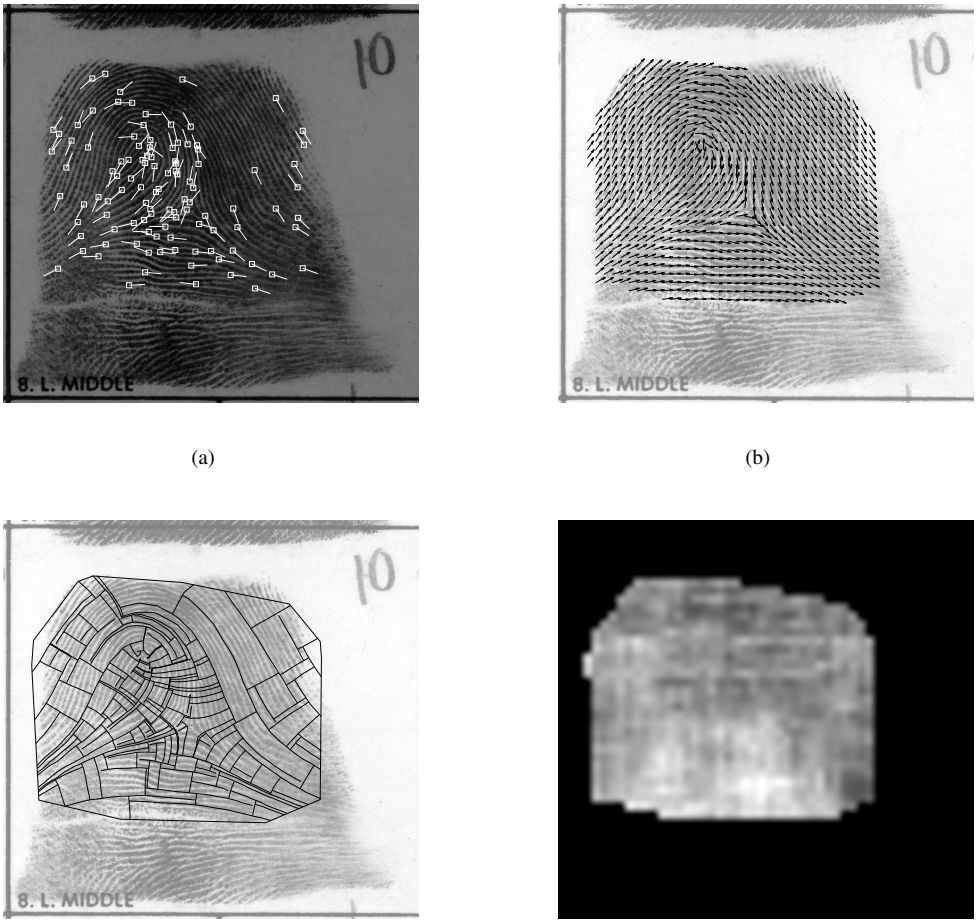

(a) (b) (c) (d)

Figure 6. The image sequence from (a) to (d) represents the median results of the proposed ridge frequency reconstruction algorithm. The reconstructed fingerprint image shown here is NIST SD27 'B104T8U'. (a) The minutiae superimposed on the gray-scale image; (b) The reconstructed orientation field; (c) The foreground is partitioned into non-overlapping SAs; (d) The reconstructed ridge frequency map, brighter pixels represent lower value of $f(x, y)$ defined in Equation 1.

above with the initial direction $\alpha_i + \frac{\pi}{2}$ and $\alpha_i - \frac{\pi}{2}$, respectively, coinciding with $\theta(x, y) + \frac{\pi}{2}$. The only difference is that the drawing terminates when it encounters $A^{\|+}$ or the border. The length of $A^{\perp}$ is evaluated by:

$$l(A^{\perp}) = \sum_{i=1}^{n-1} \sqrt{(x_{i+1} - x_i)^2 + (y_{i+1} - y_i)^2} \qquad (15)$$

where n is the total points of the streamline corresponding to $A^{\perp}$, $[x_i, y_i]$ is the coordinate of the i-th point. Fig.6 gives an example on the processing result of each step for the proposed algorithm.

6. Experiments

In this section, experiments are carried out to test the performance of our algorithm. The database used in the experiments is the NIST special database 27 [1]. In this database, there are 258 cases. Each case consists of a latent image and its matching tenprint image (referred to as the mate). In addition to images, this database contains characteristic features of minutiae and singular points(for tenprint images). These features identified on each image in this database were validated by as least two professional examiners at FBI. Therefore, the reported features should be considered reliable and useful as ground truth for measuring the performance of algorithms.

Considering the quality of minutiae directly affects the results of orientation field reconstruction, the minutiae tem-

plate examined by the FBI experts is used to reconstruct the ridge frequency map by the proposed algorithm. The ridge frequency maps reconstructed by the proposed algorithm, denoted by f_1 are compared with the results obtained by the algorithm proposed in [5] performed on the gray-scale images, which is served as the ground truth, denoted by f_2. The most familiar measure of dependence between two quantities is the Pearson product-moment correlation coefficient:

$$P(f_1(x,y), f_2(x,y)) = \frac{\sum_{i=1}^{N}(f_1(x_i,y_i)-\bar{f}_1)(f_2(x_i,y_i)-\bar{f}_2)}{\sqrt{\sum_{i=1}^{N}(f_1(x_i,y_i)-\bar{f}_1)^2 \sum_{i=1}^{N}(f_2(x_i,y_i)-\bar{f}_2)^2}} \quad (16)$$

where $\bar{f}$ is the mean of f and N is the total number of elements in f. The Pearson correlation is +1 in the case of a perfect positive (increasing) linear relationship (correlation), -1 in the case of a perfect decreasing (negative) linear relationship. If f_1 coincide with f_2, the Pearson correlation between f_1 and f_2 tends to approach 1, indicating high degree of linear dependence between them. Fig.7 shows the values of P for 258 cases. It can be observed that the results of proposed algorithm have a correlation coefficient of 0.46 on average, which indicates a high dependency with the ground truth.

7. Conclusion and Future Work

This paper proposed a novel algorithm for reconstructing the ridge frequency map from the minutiae template. The effect of local ridge flow orientations and minutiae on the change of ridge frequency is analyzed and quantized. The foreground area is divided into non-overlapping region, known as the Stable Areas (SAs). In each SA, the change of ridge frequency can be perfectly modeled by the local divergence of the unwrapped orientation field. The change of ridge frequency between adjacent SAs is a combinational effect of minutiae and local ridge flow orientations. The experiment results show that the ridge frequency map reconstructed from the minutiae template by the proposed algorithm are highly correlated to the ridge frequency map estimated from the gray-scale image. The proposed algorithm, however, fully depends on the reconstructed the orientation field. The improvement can be brought by proposing more robust orientation field reconstruction method, which takes the effect of singular points into account. The proposed algorithm can be further applied to tasks such as fingerprint reconstruction, improving minutiae-matching accuracy [4].

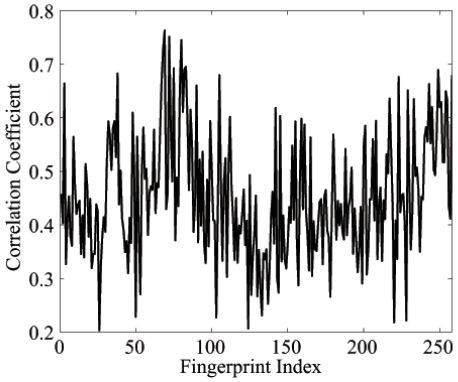

Figure 7. The Pearson correlation coefficient of the ridge frequency values.

References

[1] Nist special database 27, nist 8-bit gray scale images of fingerprint image groups (figs). http://www.nist.gov.

[2] A. M. Bazen and S. H. Gerez. An intrinsic coordinate system for fingerprint matching. *in Proc. Int. Conf. on Audio- and Video-Based Biometric Person Authentication (3rd)*, pages 198–204, 2001.

[3] R. Cappelli, A. Lumini, D. Maio, and D. Maltoni. Fingerprint image reconstruction from standard templates. *IEEE TRANSACTIONS ON PATTERN ANALYSIS AND MACHINE INTELLIGENCE*, 29(9):1489–1503, 2007.

[4] F. Chen, J. Zhou, and C. Yang. Reconstructing orientation field from fingerprint minutiae to improve minutiae-matching accuracy. *IEEE TRANSACTIONS ON IMAGE PROCESSING*, 18(7):1665–1670, 2009.

[5] S. Chikkerur, A. N. Cartwright, and V. Govindaraju. Fingerprint enhancement using stft analysis. *Pattern Recognition*, 40(1):198–221, 2007.

[6] J. Feng and A. K. Jain. Fingerprint reconstruction: From minutiae to phase. *IEEE TRANSACTIONS ON PATTERN ANALYSIS AND MACHINE INTELLIGENCE*, 13(1):234–778, 2003.

[7] C. Hill. Risk of masquerade arising from the storage of biometrics, 2001. masters thesis, Australian Natl Univ.

[8] S. Li and A. C. Kot. An improved scheme for full fingerprint reconstruction. *IEEE TRANSACTIONS ON INFORMATION FORENSICS AND SECURITY*, 7(6):1906–1912, 2012.

[9] D. Maltoni, D. Maio, A. K. Jain, and S. Prabhakar. Handbook of fingerprint recognition (second edition), 2009. Springer-Verlag.

[10] A. Ross, J. Shah, and A. K. Jain. From template to image: Reconstructing fingerprints from minutiae points. *IEEE TRANSACTIONS ON PATTERN ANALYSIS AND MACHINE INTELLIGENCE*, 29(4):544–560, 2007.

[11] B. Sherlock and D. Monro. A model for interpreting fingerprint topology. *Pattern Recognition*, 26(7):1047–1055, 2001.

[12] V. Verma, D. Kao, and A. Pang. a flow-guided streamline seeding strategy. *Proc. Conf. Visualization*, pages 163–170, 2000.

[13] P. R. Vizcaya and L. A. Gerhardt. A nonlinear orientation model for global description of fingerprints. *Pattern Recognition*, 29(7):1221–1231, 1996.